Title : will be set by the publisher
Editors : will be set by the publisher
EAS Publications Series, Vol. ?, 2002

SCIENCE WITH DIFFERENTIAL PHASES

Ph. Stee[1] and A. Domiciano de Souza Jr[1]

Abstract. Interferometry in the visible now provides milliarcsecond spatial resolution and thus has been intensely used for studying the circumstellar environment of evolved and pre-sequence stars. Up to now, most of the scientific results were obtained using only the modulus of the visibility as a function of baseline, time or projected baseline (the so-called "super-synthesis" effect). In this paper we will try to show that even without images, the phase of the visibility is able to put very strong constraints on stellar modeling since it is possible to achieve μarsecond measurements using this technique. We will illustrate through two examples from the GI2T interferometer how the modulus and the phase of the visibility were used to understand the physics of Be disks. We will stress on the importance and the potential of coupling high angular resolution with high spectral resolution for the study of stellar physics. Finally, We will present a possible study on the phase signatures due to stellar rapid rotation that can be done using the VLTI interferometer.

1 Introduction

The interferometric information delivered for astrophysical studies is the fringes visibility (V) which is a complex quantity, i.e. $V = |V| \exp^{i\phi}$. In the quasi monochromatic case, the modulus of the complex degree of coherence of the source is equal to the modulus of the normalized spatial Fourier transform of the source's brightness. Thus the visibility modulus can be written as:

$$|V| = \frac{|\tilde{O}(\vec{f})|}{|\tilde{O}(0)|} \tag{1.1}$$

[1] Observatoire de la Côte d'Azur
Département Fresnel - CNRS
Site de Roquevignon - Avenue Copernic
06130 Grasse - France

DOI: (will be inserted later)

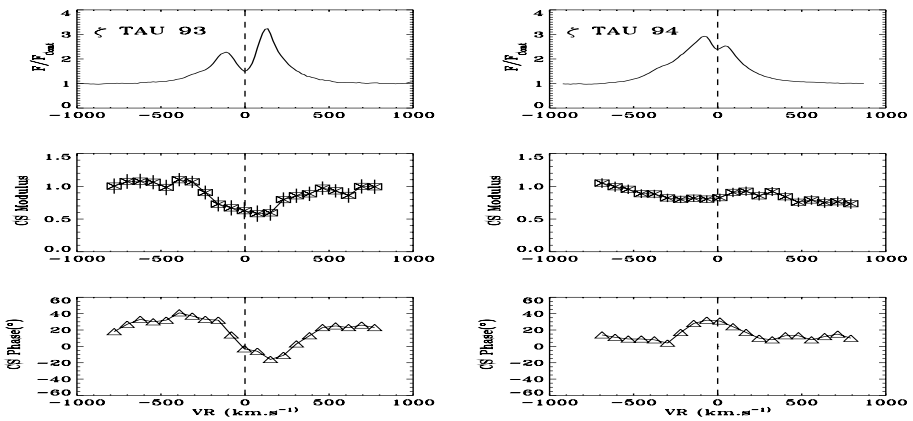

Fig. 1. Phase of the visibility as a function of wavelength

which corresponds to the contrast of the interference fringes:

$$|V| = \frac{I_{max} - I_{min}}{I_{max} + I_{min}} \tag{1.2}$$

The phase of the visibility is related to the source photocenter position onto the skyplane (see Figure 1). For instance, for a Be star, if you chose the continuum emission as a reference source (which is not really the best reference since the envelope can contribute up to 20% of the total continuum emission, see Stee et al. 1994) you can nevertheless follow the photocenter displacement as a function of the doppler shift across the Hα line profile at different epochs.
In the (X-λ) mode, used specially on the GI2T (see next section), the fringes are dispersed by a grating spectrograph in the horizontal direction and it is thus possible to combine high angular resolution ($\sim$ 1 mas) and medium spectral resolution ($\sim 1\mathring{A}$).

2 Importance of the visibility's phase: two examples from the GI2T interferometer

The GI2T/REGAIN interferometer is a Michelson interferometer with two 1.5m telescopes on a single north-south baseline between 12.0 and 65.0 m located at Caussols (France) (see Mourard *et al.* 1994a, 1994b and 1998) for a detailed description of the instrument). This instrument uses the dispersed fringes technique (X-λ mode) which allows to combine an angular resolution of $\sim$ 1 mas in the visible and a spectral resolution of $\sim$ 1 $\mathring{A}$. Thus it is possible to study the size of an emitting region at different wavelengths but also within a given spectral line, following the modulus and/or the phase of the visibility as a function of wavelength and/or time.

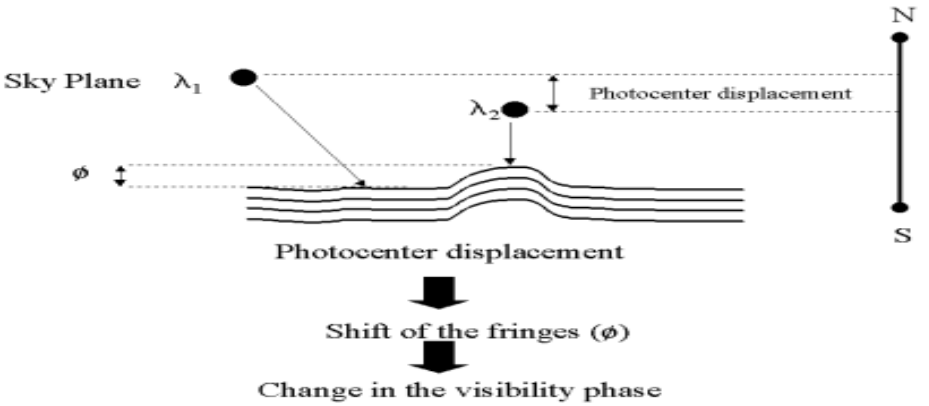

Fig. 2. Hα GI2T profiles (top) versus Doppler-shift for 93 and 94 observations of ζ Tau. Fringe amplitude and phase diagrams (Cross Spectrum Modulus middle and Cross Spectrum Phase bottom). By courtesy to F. Vakili

3 First exemple of phase as a function of time study: "One-armed" oscillations in the Be Shell star ζ Tau

Using GI2T's dispersed fringes data, Vakili *et al.* (1998) derived the relative modulus and phase of the fringe signal across Hα for 0.34 nm spectral channels by steps of 0.17nm starting from the blue and finishing in the red continua next to Hα. The relative modulus and phase diagrams are plotted in Figure 2 as a function of Doppler-shift across Hα in '93 and '94. As explained before, the relative phase diagram plotted versus Doppler-shift informs, to a first order, on the angular position of iso-radial velocity regions of the ζ Tau disk with respect to the continuum source.

From Figure 2, it can be seen that for the '93 observations the minimum fringe modulus signal estimated as (0.58±0.13) (middle-left), occurs at the same Doppler-shift as the red-maximum emission of Hα (top-left). The same remark applies to the relative phase (bottom-left) attaining its minimum value around the Doppler-shift of +130km.s^{-1}. At this Doppler shift they find a maximum deviation of (44 ± 6) deg from the average phase of continuum fringes. In terms of angular separation, computed from the fringe period λ/B=5.7 mas, this deviation yields (0.7 ± 0.1) mas to the South of the continuum source. In other words the Hα emitting region of ζ Tau at RV=130km.s^{-1} has a N-S projected position of (3.6 ± 0.5) photospheric radii to the South of the central star.

They conclude that these results are compatible with a high density pattern occuring around a radial velocity of +130 kms^{-1} and with a north-south projection position of 0.7 mas to the south of the continuum source (i.e at 3.6 R$_*$). For October 94, this density pattern has rotated prograde and occurs at a radial velocity of -70 kms^{-1}. It was now located at 0.5 mas to the north of the contiuum

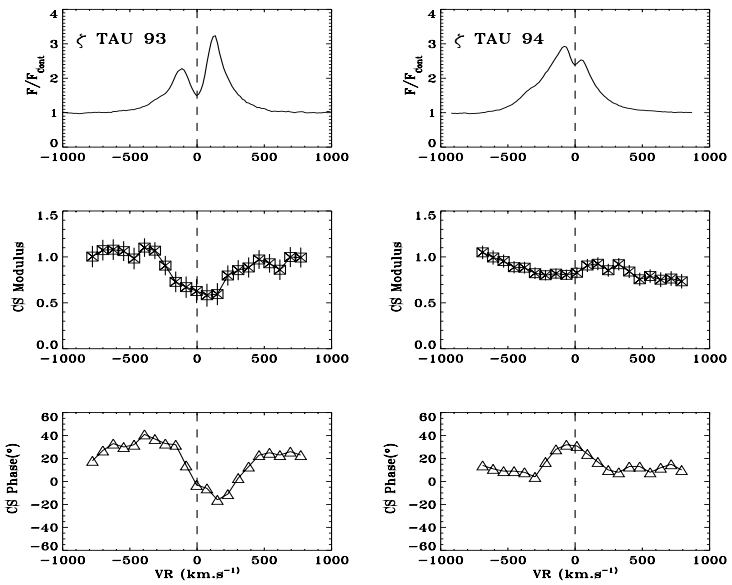

Fig. 3. Schematic representation of ζ Tau Hα long term variability (Vakili, with permission)

source which corresponds to 2.6 R_*. These observations were the first detection of an axi-asymmetric envelope around a Be star that was interpreted as a direct evidence for a prograde one-armed oscillation of its equatorial disk (see Figure 3 for a schematic representation of ζ Tau Hα long term variability).

4 Second example of phase as a function of time: "One-armed" oscillations in the Be star γ Cas

The same kind of study was done by Berio *et al.* (1999) for the Be star γ Cas. They have computed the relative phase of the fringe signal between narrow spectral channels across Hα and its neighbouring continuum for bandwidths of 0.4nm and 3nm on average respectively. They swept the Hα spectral region from the blue to the red wings by steps of 0.2nm. As for ζ Tau, the relative phase measures the spatial location (projected on the GI2T North-South baseline) of iso-radial velocity regions emitting at a given Doppler-shift with respect to the γ Cas continuum source. A positive (negative) relative phase indicates a position at the north (south) of the central star. Of course the super-resolution power of cross-spectral density method applies as long as the star is partially resolved (Chelli 1995). In figure 4 they present γ Cas relative phase as a function of Doppler-shift across Hα for different epochs of observation in '88, '91, '93 and '94. The same

diagram for the reference star α Cep observed in 1994 is plotted in figure 5 showing a nearly constant relative phase whatever the radial velocity and in agreement with an unresolved objet.

The shape of relative phase diagrams in figure 4 can directly inform us about the kinematics in the equatorial disk of γ Cas. For a rotating-expanding envelope with azimuthal symmetry (Stee 1994) the phase diagram is strictly an odd function of Doppler shift across Hα around the Radial Velocity RV=0 km.s^{-1}. Any deviation from such a shape, e.g. position of the zero phase on the Doppler-shift axis or the difference between the amplitudes of the negative and positive parts of the phase diagram implies asymetrical morphological structures in the equatorial disk of γ Cas. This is exactly what is witnessed by the phase diagrams of figure 4 for different epochs of GI2T observations: whenever V/R<1 the zero value of the relative phase occurs at negative radial velocities whilst for V/R>1 in '88 it occurs at a positive radial velocity.

Telting *et al.* (1994) have explained the V/R variations of γ Cas as resulting from global one-armed oscillations of its equatorial disc (Okazaki 1991). Such cyclic oscillations create low and high density precessing regions inside the disk with axially symetrical positions around the central star. According to this picture, the wind particles in the enhanced-density regions approach the observer for epochs where $V/R > 1$, and recede when $V/R < 1$. In order to compute the center of gravity of given iso-radial velocity regions of the disk (i.e. those parts which emit at a same Doppler-shift across Hα), they have taken into account the perturbations introduced in the density structure patterns. Assuming that these centers of gravity coincide with the photometric centers of emitting regions they can assert that:

- the photocenters of γ Cas plus its high density regions are shifted outward the central star.

- the photocenters of γ Cas plus its low density regions are shifted toward the central star.

Naturally the location of these photocenters follow the precession of the density patterns explaining in turn those of the relative phase diagram for the different observations. Finally, for different epochs of GI2T observations they find that the zero of the phase diagrams occur at +92 km s^{-1} in '88, -99 km s^{-1} in '91, -135 km s^{-1} in '93 and -38 km s^{-1} in '94. On regard of the V/R cyclic variability, these radial velocities and their temporal sequence occurence are consistant with the precession of a low density pattern having precessed in the equatorial disk of γ Cas.

After ζ Tau, γ Cas was the second Be star for which interferometric observations directly evidence a prograde one-armed oscillations of its equatorial disk (see

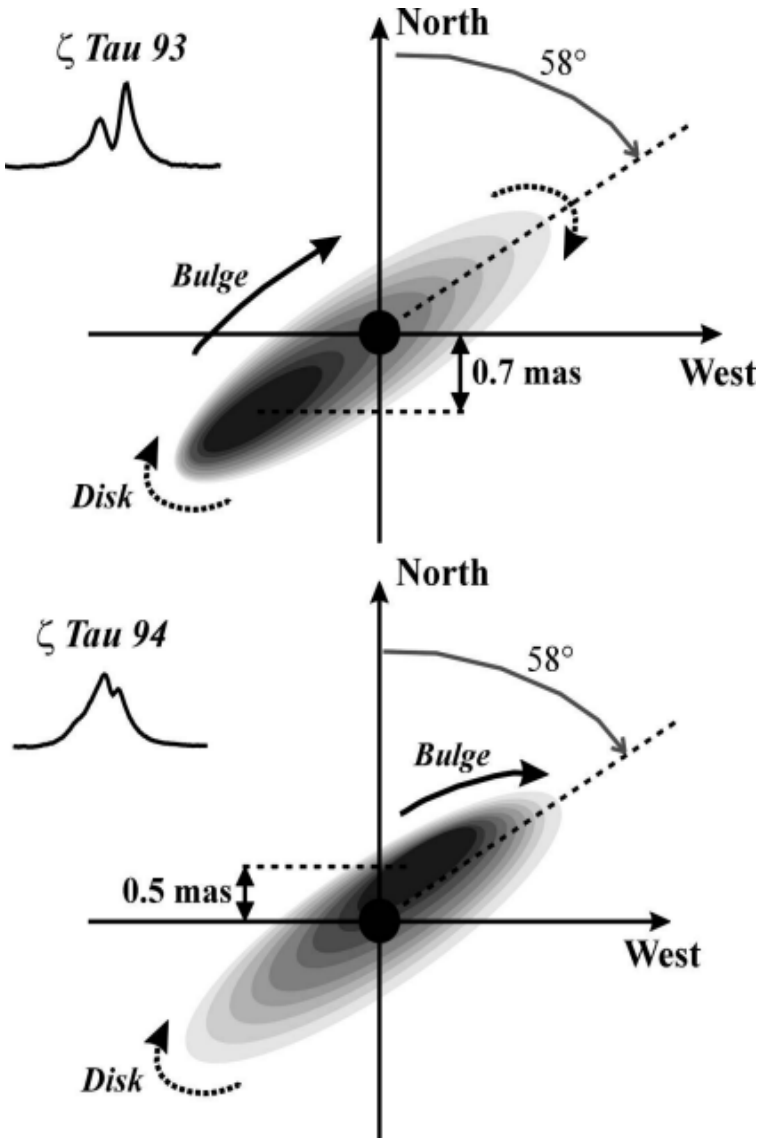

Fig. 4. Relative phase of the interferometric signal as a function of radial velocity across Hα for γ Cas observations: 88/29/12 (B=21.05m), 91/21/8 (B=49.9m), 93/8/11 (B=20.7m) and 94/6/9 (B=22.05m). The error bars are $\pm$2.5 deg. By courtesy Ph. Berio

Figure 6). This prograde precesssion agrees with the Okazaki's model (Okazaki 1997) of the one-armed (m=1) oscillation confined by the radiative effect.

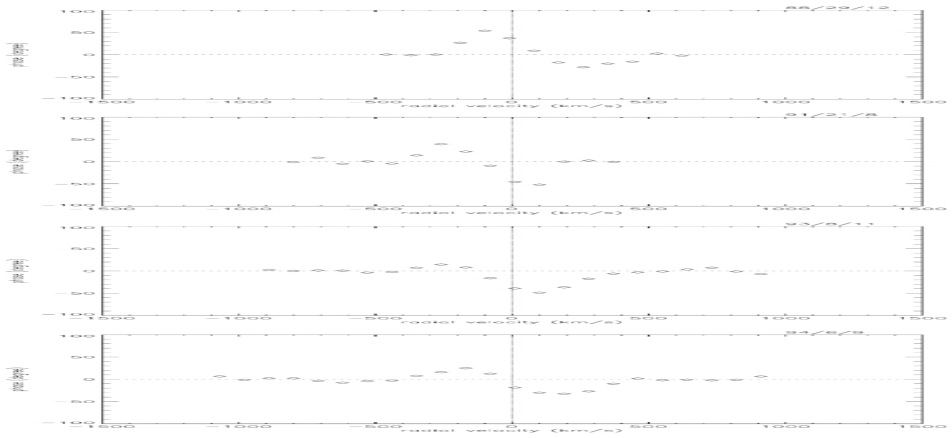

Fig. 5. Relative phase of the interferometric signal as a function of radial velocity across Hα for the reference star α Cep: 94/7/9 (B=22.05m). The error bars are $\pm$2.5deg. By courtesy Ph. Berio

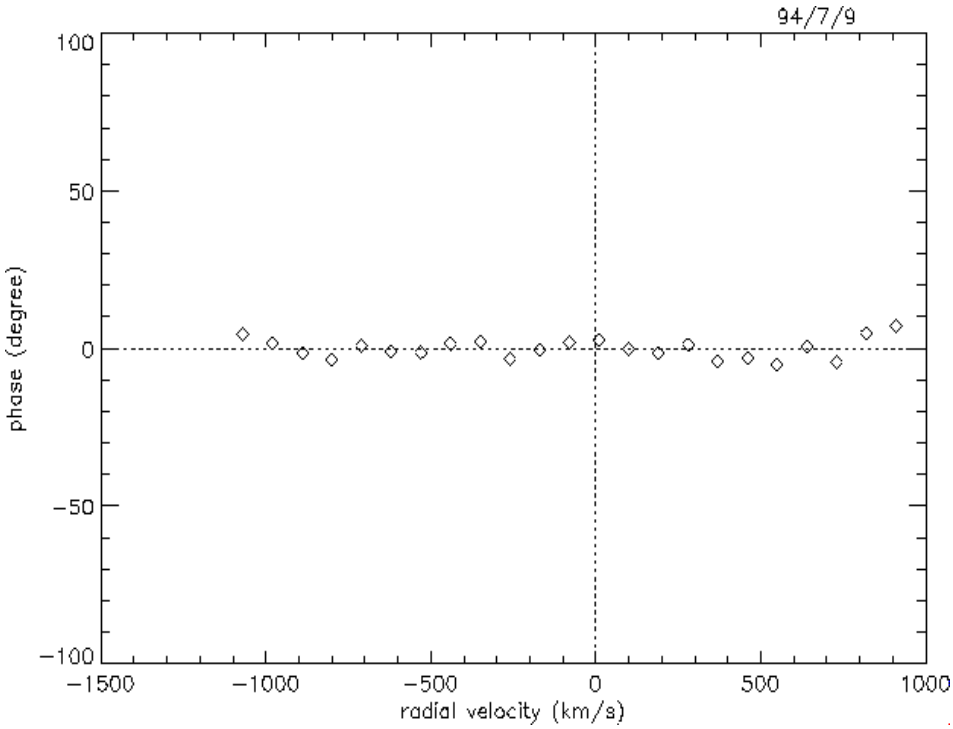

Fig. 6. Schematic representation of γ Cas one-armed precessing oscillations, confined in its equatorial plane at 1.5 R_* according to GI2T observations. The longitude of the pattern is indicated for different observation epochs. By courtesy Ph. Berio

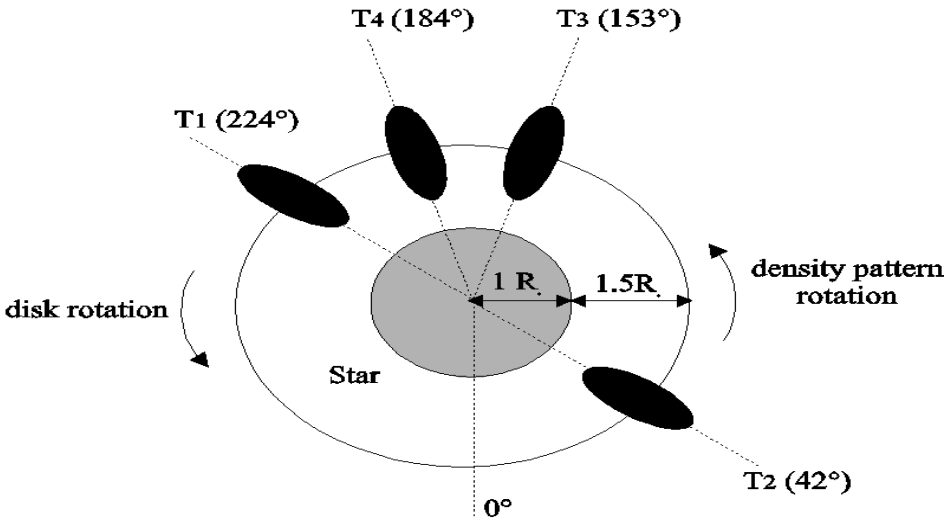

Fig. 7. Photocenter displacement of γ Cas obtained at the 6 m telescope in December 1996 using differential speckle interferometry. By courtesy Petrov R., Vassyuk V., Sanchez L. *et al.* private comm.

5 Differential speckle interferometry: a phase as a function of wavelength study

In the previous section we have studied the phase or photocenter variation as a function of time. It is also possible to study the variation of the phase at a given date but for different wavelengths. In Figure 7 we can see the photocenter displacement of γ Cas as a function of wavelength in the Hα emission line. The observations were made at the Russian 6 m telescope (resolution limit 23 mas) in December 1996 using differential speckle interferometry. The photocenter displacement show in Figure 7 is absolutely incompatible with any axisymetric model of the star enveloppe. Inside the line, the displacement shows a 1 to 2 mas structure with a North- North West privileged direction, corresponding to the direction of maximum enveloppe extension and perpendicular to the polarisation axis (Petrov R. Vassyuk V., Sanchez L. *et al.* private communication).

6 An interesting study with the VLTI interferometer: Phase signatures due to rapid rotation

Fast rotation is expected to affect stellar shapes, polarizations, temperature, gravity and brightness distribution, etc. Since stellar interferometry is a technique specially sensitive to sky projected shapes and brightness distributions, it allows a

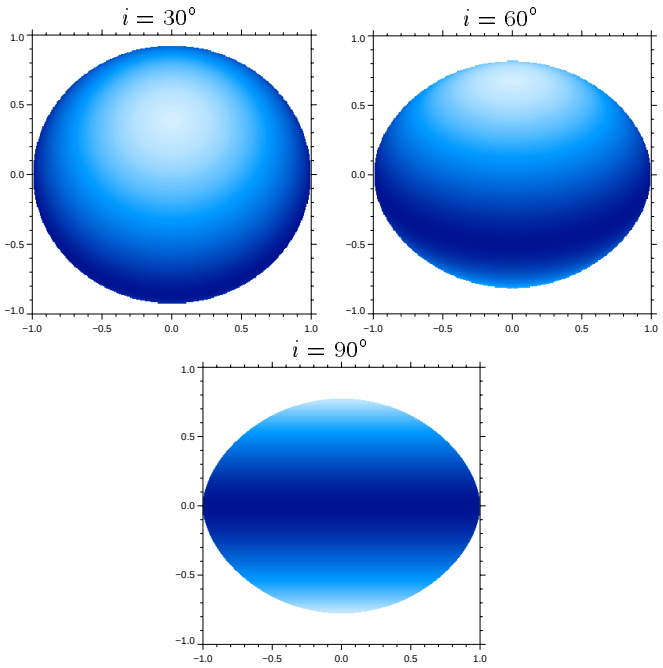

Fig. 8. Effective temperature maps for $D = 0.78$, $\beta = 0.25$ and different inclinations, with D=$\frac{R_p}{R_{eq}}$. The polar (maximum) and equatorial (minimum) effective temperatures are $T_{\rm p} = 35\,000$ K and $T_{\rm eq} = 25\,100$ K, respectively. Abscissas (y) and ordinates (z) are normalized by the angular equatorial radius $\rho_{\rm eq}$. Note that the projected geometrical deformation increases with higher inclinations but the stellar size in the y direction is constant. Since the local radiative surface flux is defined by $F(\theta) = \sigma T_{\rm eff}^4(\theta)$ this figure gives and idea of the projected brightness changes from pole to equator.

direct study of geometrical deformation and gravity darkening induced by rotation (see Figure 8). For rotating stars gravity darkening says that the local emitted flux is proportional to the local gravity g, or alternatively, $T_{\rm eff} \propto g^{\beta}$, where $T_{\rm eff}$ is the local effective surface temperature; the gravity darkening coefficient β is equal to 0.25 for hot rapidly rotating stars (von Zeipel 1924). A deeper interferometric study of uniform rapid rotators which includes gravity darkening and geometrical deformation is presented by Domiciano *et al.* (2002).

A description of the phase (ϕ) signatures due to fast stellar rotation is shown by Figure 9, *versus* the normalized spatial frequency ($\rho_{\rm eq} \vec{B_{\rm proj}} \lambda_{\rm eff}^{-1}$) where $\rho_{\rm eq}$ is the stellar angular equatorial radius), in the vicinity of the first minima and second maxima of the visibility curve. Calculations were carried out with different combinations of baseline position angle ξ, stellar inclination i and gravity darkening coefficient β inside a narrow spectral band centered on a continuum region close to the photospheric line HeI6678. The stellar parameters adopted for the calculations are $R_{\rm p} = 6{\rm R}_{\odot}$, $T_{\rm p} = 35\,000$K and $\log g_{\rm p} = 4.085$ dex ($\Rightarrow M = 16{\rm M}_{\odot}$)

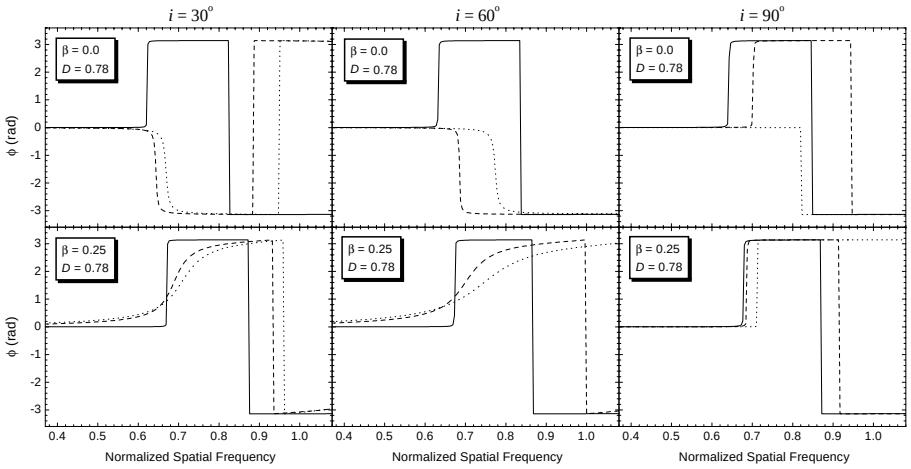

Fig. 9. Phases ϕ as a function of normalized spatial frequencies for different inclinations of a rapidly rotating star. The curves represent three different projected baseline orientations corresponding to $\xi = 0°$ (solid), $45°$ (dashes) and $90°$ (dots). See text for more details.

(see Domiciano *et al.* 2002 for further details).

The phases show significant differences between the case $\beta = 0$, where ϕ is either 0 or $\pm\pi$ rad, and the case $\beta = 0.25$ where it can take continuous values between 0 and $\pm\pi$, except when $i = 90°$ or $\xi \neq 0°$. That is because we have a non centrally symmetric intensity map resulting in phases that vary smoothly between 0 and $\pm\pi$ rad for $i \neq 0°$, $90°$ and $\xi \neq 0°$. For resolved stars these phase effects can be obtained by closure phase measurements (e.g. Young *et al.* 2000). For non resolved stars this signature in the fringe's phase could be obtained by photocenter measurements with precisions of the order of μas with phase reference techniques such as PRIMA for the VLTI (Delplancke *et al.* 2000).

7 conclusion

Through these few exemples it is clear that, even without images, the differential phase technique is a very powerful tool to investigate the shape and the behaviour of astrophysical objects as a function of time or wavelength. The forthcoming VLTI instruments AMBER and MIDI will offer such capabilities and thus will certainly bring new insights into stellar physics.

References

Barnes, T.G., Evans, D.S., 1976, MNRAS, 174, 285

Berio, Ph., Stee, Ph., Vakili, F. *et al.* , 1999, A&A, 354, 203

Chelli A., Petrov R., 1995, A&AS, 199, 389

Delplancke, F., Leveque, S., Kervella, P., Glindemann, A., DArcio, L. 2000, SPIE conference: "Astronomical Telescope and Instrumentation 2000", Munich (Germany), [4006-41]

A. Domiciano de Souza, F. Vakili, S. Jankov, E. Janot-Pacheco, L. Abe, 2002, submitted to A&A

Horagushi T., Kogure T., Hirata R. *et al.* , 1994, PASJ, 46, 9

Kogure T. and Suzuki M. 1986, Proceedings of IAU Colloq. 92, Cambridge University Press, Eds. A. Slettebak and T.P. Snow, 592

Mourard D., Tallon-bosc I., Blazit A., Bonneau D., Merlin G., Morand F., Vakili F., Labeyrie A. 1994a, A&A, 283, 705

Mourard D., Tallon-bosc I., Rigal F., Vakili F., Bonneau D., Morand F., Stee Ph. 1994b , A&A, 288, 675

Mourard, D., Thureau, N., Antonelli, P., *et al.* , 1998, SPIE Conference on Astronomical Interferometry, Vol 3350, p 517

Okazaki A.T. 1991, PASJ, 43, 75

Okazaki A.T. 1997, A&A, 318, 548

Stee, Ph., & Araújo, F.X., 1994, A&A, 292, 221.

Stee, Ph., Araújo, F.X., Vakili, F., Mourard, D., Arnold, L., Bonneau, D., Morand, F. and Tallon-Bosc, I. 1995, A&A, 301, 219.

Stee, Ph. 1996, A&A, 311, 945

Stee, Ph., Vakili, F., Bonneau, D. *et al.* , 1998, A&A, 332, 268

Telting J.H., Kapler L. 1994, A&A, 284, 515

Vakili F., Mourard D., Stee Ph., *et al.* , 1998, A&A, 335, 261.

von Zeipel, H. 1924, MNRAS, 84, 665

Young, J. S., Baldwin, J. E., Boysen, R. C., Haniff, C. A., Lawson, P. R., Mackay, C. D., Pearson, D., Rogers, J., St.-Jacques, D., Warner, P. J., Wilson, D. M. A., Wilson, R. W. 2000, MNRAS, 315, 635